Acta Pharmaceutica Sinica B 2019;9(4):819–831

Chinese Pharmaceutical Association
Institute of Materia Medica, Chinese Academy of Medical Sciences

Acta Pharmaceutica Sinica B

www.elsevier.com/locate/apsb
www.sciencedirect.com

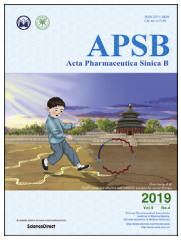

ORIGINAL ARTICLE

Multifunctional polymeric micelle-based chemo-immunotherapy with immune checkpoint blockade for efficient treatment of orthotopic and metastatic breast cancer

Jiaojie Wei, Yang Long, Rong Guo, Xinlei Liu, Xian Tang, Jingdong Rao, Sheng Yin, Zhirong Zhang, Man Li*, Qin He

Key Laboratory of Drug Targeting and Drug Delivery Systems, West China School of Pharmacy, Sichuan University, Chengdu 610041, China

Received 26 September 2018; received in revised form 11 January 2019; accepted 21 January 2019

KEY WORDS

Checkpoint blockade;
Immunotherapy;
Immunogenic cell death;
Anti-metastasis;
Nanoparticle

Abstract Immunotherapy has become a highly promising paradigm for cancer treatment. Herein, a chemo-immunotherapy was developed by encapsulating chemotherapeutic drug doxorubicin (DOX) and Toll-like receptor 7 agonist imiquimod (IMQ) in low molecular weight heparin (LMWH)-D-α-tocopheryl succinate (TOS) micelles (LT). In this process, LMWH and TOS were conjugated by ester bond and they were not only served as the hydrophilic and hydrophobic segments of the carrier, but also exhibited strong anti-metastasis effect. The direct killing of tumor cells mediated by DOX-loaded micelles (LT-DOX) generated tumor-associated antigens, initiating tumor-specific immune responses in combination with IMQ-loaded micelles (LT-IMQ). Furthermore, the blockade of immune checkpoint with programmed cell death ligand 1 (PD-L1) antibody further elevated the immune responses by up-regulating the maturation of DCs as well as the ratios of $CD8^+$ CTLs/T_{reg} and $CD4^+$ T_{eff}/T_{reg}. Therefore, such a multifunctional strategy exhibited great potential for inhibiting the growth of orthotopic and metastatic breast cancer.

© 2019 Chinese Pharmaceutical Association and Institute of Materia Medica, Chinese Academy of Medical Sciences. Production and hosting by Elsevier B.V. This is an open access article under the CC BY-NC-ND license (http://creativecommons.org/licenses/by-nc-nd/4.0/).

*Corresponding author.
E-mail address: manli@scu.edu.cn (Man Li).

Peer review under responsibility of Institute of Materia Medica, Chinese Academy of Medical Sciences and Chinese Pharmaceutical Association.

https://doi.org/10.1016/j.apsb.2019.01.018

2211-3835 © 2019 Chinese Pharmaceutical Association and Institute of Materia Medica, Chinese Academy of Medical Sciences. Production and hosting by Elsevier B.V. This is an open access article under the CC BY-NC-ND license (http://creativecommons.org/licenses/by-nc-nd/4.0/).

1. Introduction

Cancer is one of the leading causes of death worldwide, and the incidence has increased continuously. For many years, chemotherapy has been a mainstay of cancer treatment[1]. Doxorubicin (DOX), one of the most effective chemotherapeutic drugs, is essential for the treatment of a range of cancers, including lung cancer and breast cancer[2,3]. Recently, DOX has been demonstrated to activate tumor-specific immune responses by eliciting immunogenic cell death (ICD) in tumor cells, which acted as anti-cancer vaccine, and initiated powerful immune responses[4,5]. ICD could induce immune responses, which was widely accepted. Several biochemical correlates of ICD have been identified, including the exposure of calreticulin (CRT) on the surface of dying cells, and the release of large amounts of ATP and high-mobility group box 1 (HMGB1) into the extracellular milieu[6,7]. In addition, CRT exposure determines the engulfment of dying tumor cells by specific DC subsets. In this scenario, dendritic cells engulf portions of the dying cells, incorporate tumor-derived antigenic peptides into MHC molecules, and present them with adequate co-stimuli to T cells, thus stimulating the generation of tumor-specific $CD8^+$ T cells[8]. To be specific, after treatment with DOX, CRT will be expressed on tumor cell surface, which releases an "eat me" signal that induces the maturation of dendritic cells (DCs), thereby enhancing antigen presentation. Consequently, antigen-specific cytotoxic T lymphocytes (CTLs) are activated, and cytokines' secretion is also increased[9,10]. Nevertheless, the immune response induced by DOX alone is not sufficient to prevent tumor metastasis and recurrence.

It has been reported that immunotherapy can enhance the effect of chemotherapy[11,12]. Due to the ability to specifically eradicate systemic tumors and control metastases, immunotherapy emerges as an attractive approach for the treatment of cancers. Imiquimod (IMQ), a Toll-like receptor 7 (TLR7) agonist, has been proven an efficient immune adjuvant[13,14]. By triggering TLR7, IMQ induces the secretion of a variety of cytokines, and activates immune-related cells such as macrophages, dendritic cells, especially Th1 cell immunity, thereby enhancing the closely related anti-tumor ability[15–17]. Therefore, the combination of DOX and IMQ may exert synergistic anti-tumor effects by eliciting immunogenic cell death and activating antigen presenting cells. IMQ may also increase the number of CTLs and kill tumor cells consequently[18]. However, the adverse effects in the circulation of DOX and the insolubility of IMQ hindered their clinical application. Therefore, a suitable carrier which can solve these problems is urgently needed.

A self-assembled polymeric micelle was designed in this study by conjugating the hydrophilic low molecular weight heparin (LMWH) and hydrophobic D-α-tocopheryl succinate (TOS) *via* ester bonds. Our previous studies have shown that LMWH can block P-selectin-based platelet interaction with tumor cell surface mucins and inhibit epithelial–mesenchymal transition, thereby reducing metastasis[19–21]. Furthermore, TOS can reduce the expression of matrix metalloproteinase 9 (MMP9), inhibiting the degradation of stromal layer and preventing the formation of tumor micrometastasis[22–24]. It is hypothesized that the multi-functional LMWH-TOS (LT) micelles can not only be used as nanocarriers for DOX and IMQ due to their good biodegradability, but also exhibit anti-metastasis effects, contributing to the outcome of cancer therapy[25–27].

Although the elicited anti-tumor immune responses can inhibit the tumor growth, the high level of cytokines also up-regulate the expression of immune checkpoints. The interaction between programmed cell death 1 (PD-1) and its ligand PD-L1 may produce immune inhibition signals, which attenuated the tumor-specific immune responses[28]. To further enhance the anti-tumor immune responses and relieve the immunosuppression, the blockade of checkpoints offers a solution. It has been reported that immune activators may be synergistic with PD-1 pathway inhibitors such as anti-PD-L1[29–33].

In this study, we present an immune-stimulating strategy that encapsulates DOX and IMQ in LT micelles in combination with a PD-L1 checkpoint blockade to effectively suppress orthotopic 4T1 breast cancer and its lung metastases. DOX- and IMQ-loaded micelles were formulated and characterized. The cell toxicity, cell apoptosis and anti-metastasis effect of drug-loaded micelles were tested on 4T1 cells *in vitro*. Besides, the maturation of dendritic cells and activation of tumor-specific immune responses of LT-DOX+LT-IMQ in combination with anti-PD-L1 were analyzed *in vivo*. The anti-tumor and anti-metastasis effects of combined therapy were evaluated on 4T1 tumor-bearing mice. Additionally, the mechanisms of anti-tumor and anti-metastasis responses were also explored.

2. Materials and methods

2.1. Materials and animals

Low molecular weight heparin (LMWH) was obtained from Melonepharma (Dalian, China). D-α-Tocopheryl succinate (TOS) and doxorubicin hydrochloride were obtained from J&K Scientific Co., Ltd. (Beijing, China). Imiquimod was obtained from Abmole Bioscience Inc. (Houston, TX, USA). 1-[3-(Dimethylamino) propyl]-3-ethylcarbodiimide hydrochloride (EDC) and *N*-hydroxy-succinimide (NHS) were obtained from Keddia Reagent (Chengdu, China). 4-(Dimethylamino) pyridine (DMAP) was obtained from Sigma–Aldrich (St. Louis, MO, USA). PD-L1 antibody was purchased from BioXCell. Recombinant murine IL-2 was obtained from Peprotech (Rocky Hill, CT, USA). MTT, 1,1′-dioctadecyl-3,3,3′,3′-tetramethylindodicarbocyanine, 4-chlorobenzenesulfonate salt (DiD), 4,6-diamidino-2-phenylindole (DAPI) and LDH kits were purchased from Beyotime Institute Biotechnology (Shanghai, China). Anti-CD3e-PE, anti-CD4-FITC, anti-CD8a-FITC, anti-CD11c-PE, anti-CD80-FITC and anti-CD86-FITC were bought from eBioscience (San Diego, CA, USA). Matrigel was bought from BD Biosciences (San Jose, CA, USA). CRT antibody was bought from Boster Biological Technology (Wuhan, China) and secondary antibody was purchased Shanghai Abways Biotechnology Co., Ltd. (Shanghai, China). ELISA kits for IFN-γ and TNF-α, annexin V-FITC/PI apoptosis detection kit were obtained from KeyGEN Biotech (Nanjing, China). Plastic cell culture dishes and plates were purchased from Wuxi NEST Biotechnology Co. (Wuxi, China). Other reagents and chemicals were of analytical grade. BALB/c mice (about 5-week-old, 18–21g) were purchased from Dashuo Experimental Animal Company (Chengdu, China). All animal experiments were performed according to the rules of Experimental Animals Administrative Committee of Sichuan University (Chengdu, China).

2.2. Synthesis of LMWH-TOS

The amphiphilic LMWH-TOS was synthesized as described previously, by attaching TOS to LMWH through ester bond formation[21]. First, TOS (201 mg), EDC (126.5 mg), NHS

(76.0 mg) and DMAP (20.1 mg) were dissolved in *N*,*N*-dimethylformamide (DMF). The mixture was stirred for 3 h to activate the carboxylic acid groups of TOS. Meanwhile, LMWH (100 mg) was dissolved in formamide at 50 °C and added slowly into the activated TOS solution. The reaction mixture was stirred for 48 h, and then dialyzed against deionized water for 72 h and lyophilized. All the structures were characterized by ^{1}H NMR spectra using a Varian Mercury 400 NMR system (Varian Inc., Palo Alto, CA, USA) and by PerkinElmer Spectrum two FI-IR (USA).

2.3. Hemolysis assay

For the hemolysis study, fresh mouse blood was collected, and red blood cells (RBCs) were obtained after centrifugation and washed with PBS. LT with different concentrations was incubated with 2% red blood cell suspension from mouse for 2 h at 37 °C. Then, each sample was centrifuged at 3000 rpm (5427R, Eppendorf, Hamburg, Germany) for 10 min. The absorbance of supernatant was analyzed at 545 nm by a microplate reader and the precipitated erythrocytes were observed under microscope. The hemolysis (%) was calculated according to Eq. (1). A hemolysis ratio (%) of less than 5% was regarded as nontoxic.

$$\text{Hemolysis}\ (\%) = \left[A_{\text{sample}} - A_{\text{PBS}}\right] / \left[A_{\text{ultrapure water}} - A_{\text{PBS}}\right] \times 100 \quad (1)$$

PBS and ultrapure water treated erythrocyte suspensions were used as negative and positive controls, respectively.

2.4. CRT exposure

The CRT exposure after DOX treatment assessed by flow cytometry (FCM) and confocal lacer scanning microscopy. For analysis by FCM, 4T1 cells were seeded into 6-well plate at a density of 5×10^5 cells/well and allowed for attachment overnight. After 4 h incubation with LT, free DOX, LT-DOX at an equivalent DOX dose of 3 μmol/L, cells were collected and washed twice with PBS. Afterwards, cells were treated with CRT primary antibody for 1 h and then stained with secondary antibody for 30 min at 4 °C in darkness and then analyzed by flow cytometer (Cytomics FC 500, Beckman Coulter). For immunofluorescence observation, cells were seeded on slips and incubated with LT, free DOX, LT-DOX at an equivalent DOX dose of 3 μmol/L. After washed by PBS, cells with no permeabilization were stained by anti-CRT primary antibody for 1 h and then stained with secondary antibody for 30 min at 4 °C in darkness. Cells were then fixed in 4% paraformaldehyde for 15 min and nuclei were stained with DAPI for 5 min. After being washed with cold PBS three times, the coverslips were imaged by a laser scanning confocal microscope (FV1000, Olympus, USA).

2.5. Pharmacokinetics study

For the pharmacokinetic assay, female BALB/c mice (6 mice/group) were injected with free DOX&IMQ and LT-DOX+LT-IMQ (at an equivalent dose of 3 mg/kg DOX, 0.75 mg/kg IMQ) through the tail vein. Three mice were randomly chosen for the first 5 time points, and the other 3 mice were used for the remaining 5 time points. Approximately 100 μL of blood was collected in 0.5-mL heparin-treated tubes from the orbit sinus at each time point (3, 15, 30 min, 1, 2, 4, 6, 8, 12 and 24 h). The blood samples were centrifuged at 4 °C and 5000 rpm (5427R, Eppendorf) for 10 min to obtain 50 μL of supernatant plasma, and four volumes of precipitation agent (200 μL) was added to each sample. The samples were oscillated for 3 min, sonicated for 15 min, and centrifuged at 4 °C and 12,000 rpm (5427R, Eppendorf) for 10 min. The supernatant was collected and filtered through a 0.22-μm filter for LC–MS/MS analysis. The chromatographic conditions were as follows: chromatographic column, C18 (2.1 mm × 50 mm, 1.7 μm); mobile phase, 0.1% formic acid in water: methanol (*v*/*v* = 45/55). The mass spectrometer was operated in positive ion mode using an electrospray source and the quantification analysis was performed using multiple reaction monitoring, with the transition of the *m*/*z* 544.2 → *m*/*z* 397.1 for DOX and *m*/*z* 241.1 → *m*/*z* 185.0 for IMQ. The pharmacokinetic data was analyzed by Data and max Statistics (DAS, Shanghai, China).

2.6. Evaluation of in vivo immune status after different treatments

Six days after tumor implantation, animals with an average tumor volume of 80–100 mm^3 were selected and divided into 5 groups randomly (n = 3). Mice of each group received 3 i.v. injections, and were sacrificed 7 days after the last dose and their spleens were collected. Splenocytes suspensions were prepared by using the Spleen Dissociation kit (Miltenyi Biotec Germany). The extracted spleen cells were stained with anti-CD11c-PE, anti-CD86-FITC and anti-CD80-FITC, and then detected by flow cytometry.

To analyze the $CD8^+$ and $CD4^+$ T cell responses in tumors, tumors were harvested from mice in different groups and stained with anti-CD3e-eFluor 610, anti-CD8a-FITC, anti-CD4-FITC antibodies according to the manufacturer's protocols. Briefly, tumor tissues were cut into small pieces and put into a glass homogenizer containing PBS (pH 7.4) with 2% heat-inactivated fetal bovine serum. Then, the single-cell suspension was prepared with the homogenizer without addition of digestive enzyme. Finally, cells were stained with fluorescence-labelled antibodies after the removal of red blood cells (RBC) using the RBC lysis buffer.

Serum samples were isolated from mice after various treatments and diluted for analysis. Tumor necrosis factor (TNF-α) and interferon gamma (IFN-γ) were analyzed with ELISA kits according to the protocols of vendors.

2.7. Ex vivo cytotoxicity assay of cytotoxic T lymphocytes

In order to obtain the activated splenocytes as effector cell, 1×10^6 4T1 cells were orthotopically implanted into the mammary fat pad of female BALB/c mice on day 0. The average volume of tumors was approximately 100 mm^3 on day 8, the mice were divided into 4 groups randomly to receive the following treatments: Hepes, free DOX&IMQ, LT-DOX, LT-DOX+LT-IMQ. The dosages of DOX and IMQ were 3 and 0.75 mg/kg, respectively. The second treatment with the same dosing regimens was given to each group on day 11. Three days later, the mice were sacrificed and the spleens were harvested. The spleen dissociation kit (Miltenyi Biotec Germany) were utilized to prepare the solution of splenocytes, which were further incubated with mitomycin C-treated 4T1 tumor cells for 72 h at 37 °C under 5% CO_2 with mouse IL-2 added into the culture media. After stimulation, viable splenocytes were used as effector cells for the measurement of specific cytotoxicity activity. And 4T1 cells were used as target cells. The splenocytes obtained from LT-DOX+LT-IMQ group

were divided into two parts, one of which was added to 4T1 cells that had been given anti-PD-L1 in advance, while the other was added to normal 4T1 cells. The cytotoxicity of cytotoxic T lymphocytes was determined by LDH kits in accordance with manufacturer's protocol.

2.8. Therapeutic effect on 4T1 orthotopic tumor models

To further eliminate immunosuppressive factors, we combined anti-PD-L1 with LT-DOX+LT-IMQ to treat 4T1 orthotopic tumors and metastatic tumors. Five days after tumor implantation, animals with an average tumor volume of 80–100 mm^3 were selected and divided into 5 groups randomly ($n = 6$): Hepes, free DOX&IMQ, LT-DOX, LT-DOX+LT-IMQ, LT-DOX+LT-IMQ+anti-PD-L1. The mice of each group were dosed intravenously on days 6, 9, and 12, and the tumor volumes were measured with a vernier caliper every two days. According to the earlier results we obtained, the administration dosage of DOX, IMQ and anti-PD-L1 were finalized at 3, 0.75 and 2.5 mg/kg, respectively. Mice were sacrificed on day 16, and the tumors were collected for hematoxylin and eosin (H&E) and terminal dexynucleotidyl transferase (TdT)-mediated dUTP nick-end labeling (TUNEL) staining. Immunohistochemistry staining of PD-L1 was performed. Tumor growth was calculated from caliper measurements with Eq. (2):

$$\text{Tumor volume} = \left(L \times W^2\right)/2 \quad (2)$$

where L is length and W is width.

2.9. Therapeutic effect on lung metastatic tumor models

To establish lung metastasis model of breast cancer, mice were intravenously injected with tumor cells on day 1. Five days later, mice were randomly divided into 7 groups ($n = 5$), and injected with Hepes, LMWH, LT, free DOX+IMQ, LT-DOX, LT-DOX+LT-IMQ, LT-DOX+LT-IMQ+anti-PD-L1, respectively. The administration dosages of DOX, IMQ and anti-PD-L1 were 2.5, 0.75 and 2.5 mg/kg, respectively. The dosing interval between LT-DOX+LT-IMQ and anti-PD-L1 was 48 h. The treatment was conducted every 3 days for 3 times. On day 23, mice were euthanized, and lung tissues were collected. The macroscopic tumor nodules on the whole surface were counted. Immunohistochemistry staining of MMP9 was also performed.

2.10. Statistical analysis

All the data were presented as mean ± standard deviation. Statistical comparisons were performed by one-way ANOVA for multiple groups. P values < 0.05 were considered statistically significant.

3. Results

3.1. Synthesis and characterization of drug-loaded micelles

LMWH was conjugated to the TOS *via* ester bonds. The successful synthesis of LMWH-TOS was confirmed by ^{1}H NMR (Supporting information Fig. S1) and infrared spectroscopy (Supporting information Figs. S2–4). Since LMWH could bind to toluidine blue, quantification of the content of LMWH in LT conjugate was then determined by analyzing the dissociated toluidine blue at 629 nm. The result showed that the content of LMWH in LT was 29.2%, *w/w* (Supporting information Fig. S5). The loading capacities of DOX and IMQ in LT-DOX and LT-IMQ micelles were ~8.1% and ~5.2%. (Supporting information Table S1). The average hydrodynamic size of LT-DOX was 133.9±2.8 and LT-IMQ was 112.7±1.5 nm (Table S1). Both LT-DOX and LT-IMQ exhibited uniform and spherical appearance under TEM observation (Fig. 1A and B, inset).

It has been reported that heparin has anticoagulant function, which may increase the hemolytic activity of LT and lead to corresponding side effects[34]. The hemolysis of LT was lower than 3% when the concentration ranged from 100 to 900 μg/mL (Fig. 1C and D). Microscopic examination and photographs showed that after co-incubation with LT, no structure change of the erythrocyte membrane or aggregation of red blood cells were observed, which was similar to the results of PBS-treated group (negative control, Supporting Information Fig. S6). All the results confirmed that LT micelle exhibited little hemolytic effect.

The sizes of three nanoparticles in 50% FBS showed little change over 48 h (Fig. 1E). Meanwhile, no obvious changes were observed in the serum turbidity for all three nanoparticles (Fig. 1F). Cumulative release of DOX and IMQ from LT-DOX and LT-IMQ were investigated in PBS. As shown in Fig. 1G, approximately 75% of the total DOX was released after incubation at pH 5.0 for 48 h, while approximately 39% DOX was released at pH 7.4. After 48 h's incubation, the release of IMQ at pH 7.4 and pH 5.0 were ~20% and ~40%, respectively, indicating that the release of DOX and IMQ in acidic medium was increased.

3.2. Cytotoxicity and apoptosis assays

The cytotoxicity was measured by MTT assays. Both free DOX and LT-DOX exhibited enhanced anti-proliferation effects as drugs concentration increased. The cell inhibition of DOX plus IMQ was higher than that of LT-DOX plus LT-IMQ. In addition, LT almost did not affect cell viability on 4T1 cells. Even if the concentration of the LT was as high as 500 μg/mL, no obvious cytotoxicity was observed (Supporting Information Fig. S9).

The cell apoptosis induced by drug-loaded micelles was detected by annexin V-FITC/PI assay. The percentage of apoptosis and necrotic cells was 6.8±0.59% for Hepes, 85.1±0.34% for free drugs, 59.9±1.57% for LT-DOX, 28.3±1.96% for LT-IMQ and 61.7±1.20% for LT-DOX+LT-IMQ, respectively (Fig. S9).

3.3. In vitro anti-metastatic effect

Our previous studies have verified that LMWH could inhibit the adhesion between tumor cells and platelets and TOS could inhibit the production of MMP9, thereby inhibiting different phases of the metastasis cascade[20,21]. Thus, the *in vitro* anti-metastatic effects of micelles were evaluated. Firstly, wound healing assays were used to assess the inhibitory effect of micelles. The healing rate of control group was approximately 80%. The healing abilities of LT-treated and free DOX&IMQ-treated groups were similarly reduced. Notably, LT-DOX plus LT-IMQ group significantly reduced the cell motility compared with LT, LMWH and free drugs groups, reducing the wound closure rate to less than 20% (Fig. 2A and B).

Furthermore, invasion assays were performed *in vitro*. As can be seen in Fig. 2C and D, cells treated with Hepes buffer could easily invade into the lower chamber. For the LT-treated group,

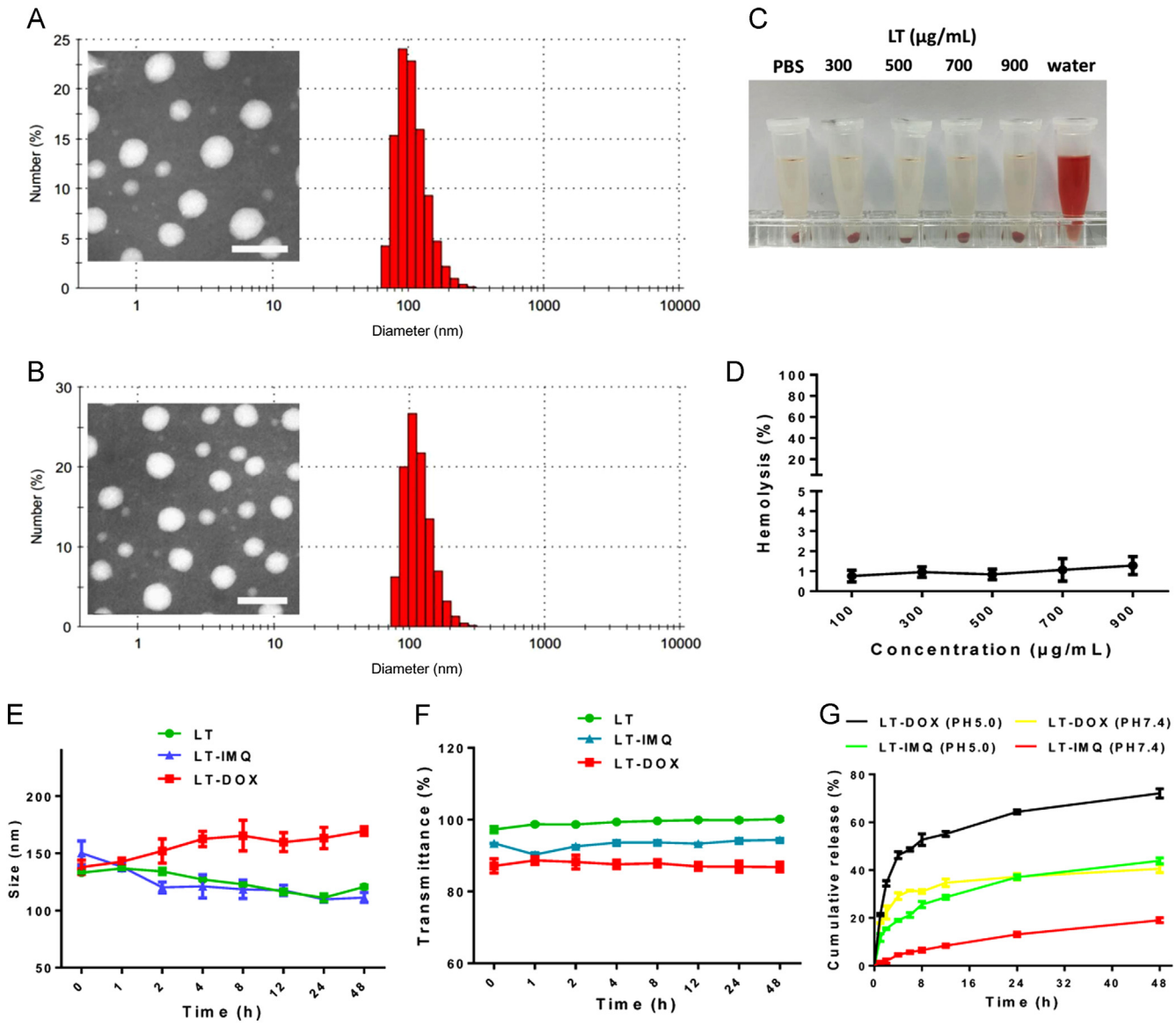

Figure 1 Hydrodynamic diameters and TEM image of (A) LT-DOX and (B) LT-IMQ. (C) Photo images of plastic pipe containing supernatant from red blood cell content treated with different concentrations of LT. (D) Hemolysis (%) of red blood cell cultured with LT at various concentrations. Less than 5% hemolysis was regarded as nontoxic. (E) Stability of nanoparticles represented by size when incubated in 50% FBS for 48 h at 37 °C. (F) The turbidity variation (represented by transmittance) of nanoparticles in 50% FBS. (G) *In vitro* release kinetics of DOX and IMQ from micelles of LT-DOX and LT-IMQ.

the number of cells in the lower layer was greatly reduced compared with Hepes and LMWH treated group. Similarly, free DOX&IMQ also reduced the number of invaded cells, probably owing to the cytotoxicity. When treated with LT-DOX + LT-IMQ, the number of cells passing through the membrane was significantly lowest, only one-tenth that of the control group ($P<0.001$). Therefore, LT-DOX plus LT-IMQ could effectively inhibit the migration and invasion ability of 4T1 cells *in vitro*.

3.4. *CRT exposure induced by DOX and pharmacokinetic properties*

DOX could engage a tumor-specific immune response by inducing immunogenic cell death (ICD)[35,36]. Calreticulin (CRT) acts as the "eat me" signal and promotes the phagocytosis, regulating DC-mediated tumor antigen cross-presentation and T cell polarization[37]. Flow cytometry results showed that the expression of CRT on the surface of cancer cells treated with DOX or LT-DOX was significantly increased (Fig. 3A). The immunostaining analysis was consistent with the flow cytometry results (Fig. 3B). With the help of adjuvant LT-IMQ, the immunogenic signal of CRT may consequently induce potent immune responses against tumors *in vivo*. Pharmacokinetics studies of micelles were performed in BALB/c mice. Plasma concentration–time curves of free DOX&IMQ and LT-DOX+LT-IMQ after intravenously administration were shown in Fig. 3C and D. As expected, free DOX and IMQ showed a higher clearance *in vivo*. At 2 h post-injection, the free drugs concentrations of free drug group was already under the limit of detection. In contrast, LT-DOX and LT-IMQ showed

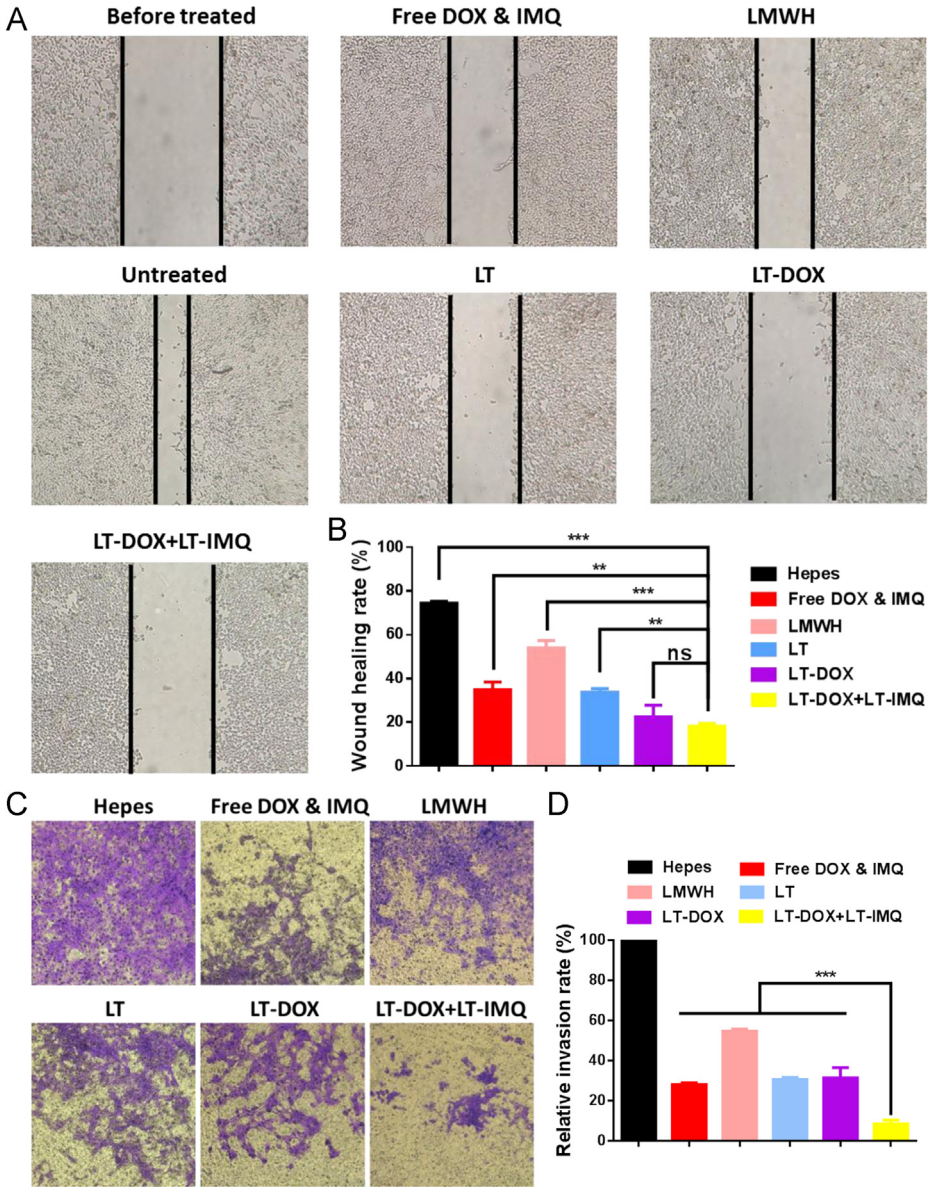

Figure 2 (A) Representative images of healing extent treated with different preparations after 24 h. (B) Wound healing rate. (C) Representative images of invaded 4T1 cells when treated with different formulations for 48 h. (D) Relative invasion rate of invaded cells. Data are mean ± SD, $n = 3$; $^{*}P < 0.05$; $^{**}P < 0.01$; and $^{***}P < 0.001$.

much higher concentration at all-time points. Pharmacokinetic parameters were shown in Supporting Information Table S2. LT-DOX and LT-IMQ significantly decreased clearance rate and enlarged AUC_{0-t} and $AUC_{0-\infty}$.

3.5. *In vivo immunity level after treatment*

After intravenous injection of DiD-loaded micelles (LT-DiD) into 4T1 tumor-bearing mice, the bio-distribution was detected by the IVIS imaging system. Fluorescence can be observed at the tumor site 2 h after the injection (Supporting Information Figs. S10 and S11), and the fluorescence intensity was increased over time through EPR effect. We speculated that LT-IMQ could induce a strong immune response *in vivo* as an adjuvant, which also enhanced the immune activation of LT-DOX. To verify this hypothesis, 4T1 orthotopic tumor bearing mice were intravenous injected with Hepes, free DOX&IMQ, LT-DOX, LT-DOX+LT-IMQ or LT-DOX+LT-IMQ+anti-PD-L1. Three days post injection, mice were sacrificed and the spleens were collected for flow cytometry analysis after co-staining with CD11c (the DC marker), CD80 and CD86 (Fig. 4A and B). Compared with LT-DOX and free drugs treated groups, the maturation of DCs of LT-DOX+LT-IMQ treated group increased by 2.4- and 1.5-fold, respectively. Moreover, after combination with anti-PD-L1, the percentages of mature DCs further increased by 1.3-fold (Fig. 4C and D). The high expression of PD-L1 on DC cells might suppress the maturation of DCs. After combination with anti-PD-L1, the negative effects were eliminated, which enhanced the activity of DC cells[38,39]. The results were consistent with the *in vitro* BMDC maturation results (Supporting information Fig. S8).

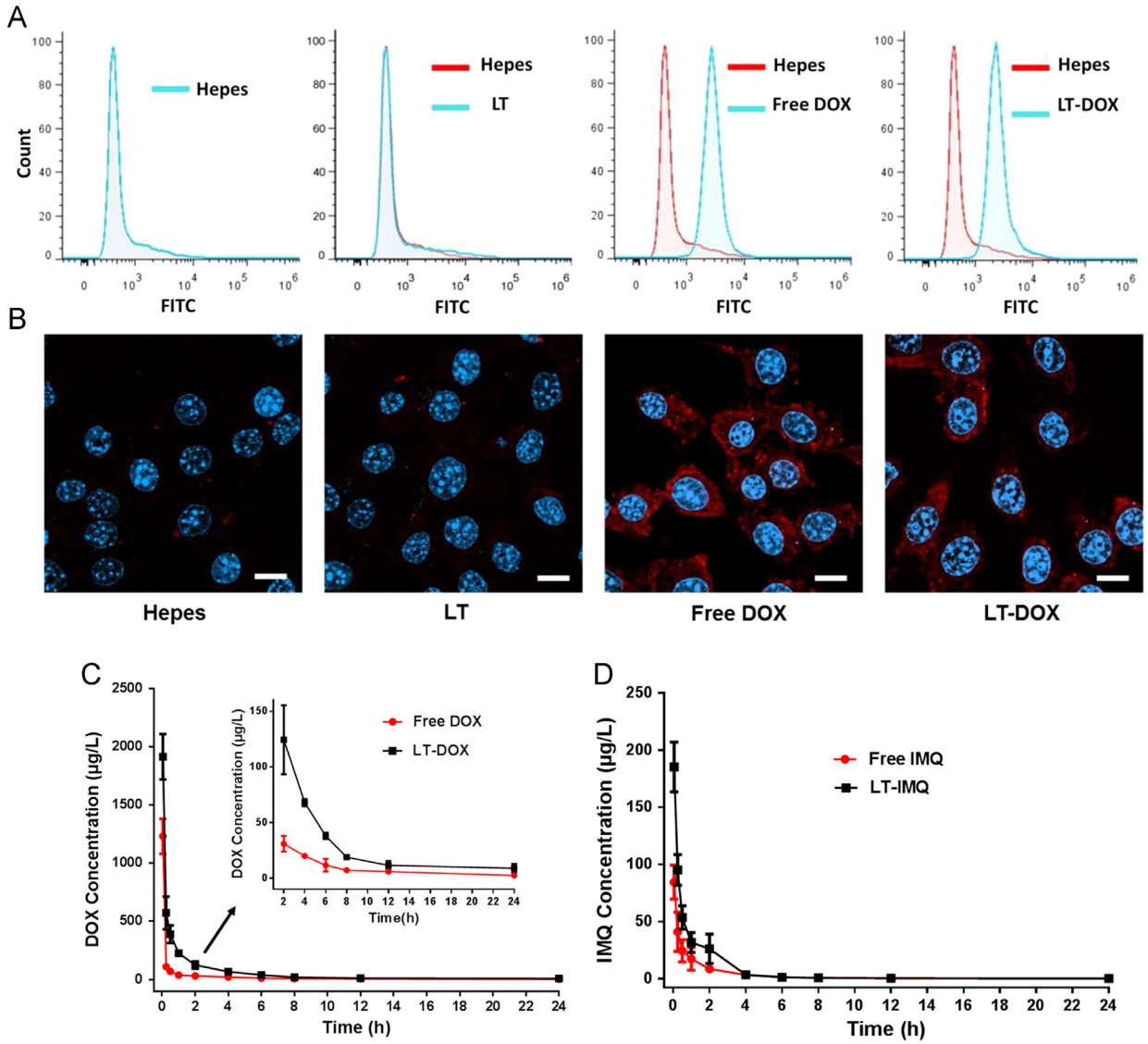

Figure 3 (A) CRT exposure on the cell surface of 4T1 cells was evaluated by flow cytometry after different treatments. (B) Immunofluorescence microscopy of CRT expression on the cell surface of 4T1 cells after different treatments. The scale bar represents 10 μm. (C) and (D) DOX and IMQ plasma concentration–time profiles in BALB/c mice treated with different DOX and IMQ formulations (at a dose of 3 mg/kg DOX, 0.75 mg/kg IMQ; data are mean ± SD, $n = 3$).

To better understand the mechanism of synergistic anti-tumor effect triggered by LT-DOX+LT-IMQ in combination with anti-PD-L1 therapy, the tumor-infiltrating T cells were studied. $CD8^+$ T cell-mediated cytotoxicity is a crucial step in tumor immunotherapy. This process not only requires DC cells to effectively present tumor antigens to cytotoxic T lymphocytes cells, but also needs corresponding cytokines which are secreted by helper T cells to promote CTLs production[40,41]. The activation of antigen-specific $CD8^+$ CTLs and $CD4^+$ T cells were examined. The tumors from Hepes treated mice clearly showed limited T cell (~1.00% for $CD4^+$, ~1.24% for $CD8^+$ cells) infiltration (Fig. 5A, B, D, E). In comparison, after combined treatment of LT-DOX+LT-IMQ and anti-PD-L1, the number of infiltrating $CD8^+$ and $CD4^+$ T cells were remarkably increased, which was beneficial for the anti-tumor effect. $CD4^+$ helper T cells ($CD3e^+CD4^+$) can be divided into effective T cells that are helpful to promote immune responses and regulatory T cells (T_{reg}, $CD4^+Foxp3^+$) which could hamper effective anti-tumor immune responses. Compared with other groups, although immune responses have been also generated after LT-DOX treatment, the anti-tumor efficacy in this group remained less effective owing to the presence of high percentages of T_{reg} cells. As illustrated in Fig. 5C and F, the number of T_{reg} cells was significantly reduced with PD-L1 blockade. However, the ratios of $CD8^+$ CTLs/T_{reg} cells and $CD4^+$ T_{eff}/T_{reg} cells of LT-DOX+LT-IMQ plus anti-PD-L1-treated group were increased to nearly 2-fold compared with LT-DOX+LT-IMQ-treated group, and more than 3-fold compared with Hepes, free drugs and LT-DOX-treated groups, indicating stronger cellular immune responses in cancer immunotherapy (Fig. 5G).

Cytokine secretion in tumor microenvironment was important to tumor growth as well. The secretion level of TNF-α and IFN-γ play an important role in T-helper cell 1 type (Th1) immune response[42,43]. Cytokines secretions induced by LT-DOX+LT-IMQ plus

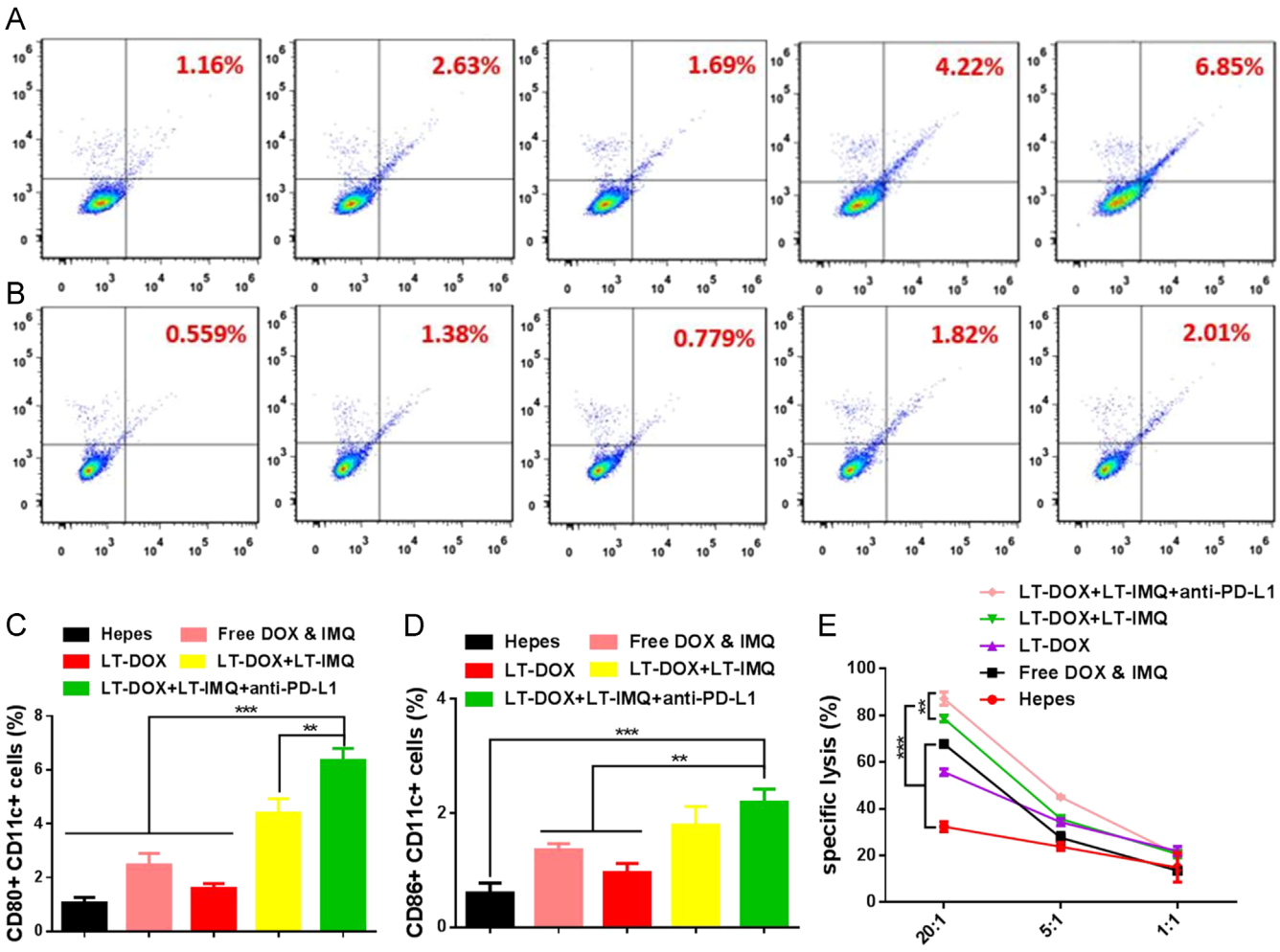

Figure 4 The expression status of $CD80^+$ and $CD86^+$ on $CD11c^+$ dendritic cells from spleens. Representative flow cytometry plots showing percentages of $CD11c^+CD80^+$ cells (A) and $CD11c^+CD86^+$ cells (B). From left to right are groups of Hepes, free DOX & IMQ, LT-DOX, LT-DOX+LT-IMQ, LT-DOX+LT-IMQ+anti-PD-L1. Proportions of $CD11c^+CD80^+$ cells (C) and $CD11c^+CD86^+$ cells (D). (E) The cytotoxicity assay of $CD8^+$ T lymphocytes against 4T1 cells. Data are mean ± SD, $n = 3$; $^*P < 0.05$; $^{**}P < 0.01$; and $^{***}P < 0.001$.

anti-PD-L1 were obviously higher than the rest groups, which was helpful for triggering anti-tumor immune response (Fig. 5H and I).

3.6. *Ex vivo cytotoxic T lymphocytes responses*

To further ascertain the function of CTLs, we conducted an *ex vivo* CTLs response assay. As shown in Fig. 4E, the effector cells extracted from the mice treated with LT-DOX+LT-IMQ showed a strong killing effect on 4T1 cells. Moreover, after pre-treatment with anti-PD-L1, the killing effect of $CD8^+$ T cells obtained from LT-DOX+LT-IMQ group was significantly elevated (Fig. 4E). When the ratios of effector cells: tumor cells were 20:1 and 5:1, anti-PD-L1 could significantly increase the killing effect of the effector cells on tumor cells ($P < 0.01$). However, when the ratio of effector cells: tumor cells was 1:1, no significant difference was observed between groups, indicating that anti-PD-L1 increased the cytotoxicity of effector cells not by direct killing, but by blocking the inhibitory signals of tumor cells.

3.7. *Anti-tumor and anti-metastasis efficacy in vivo*

In the animal experiments, aiming at enhancing the anticancer therapeutic efficacy of chemo-immunotherapy, PD-L1 blockade therapy was introduced. In this section, we evaluated the therapeutic effect of combined therapy on 4T1 tumor bearing BALB/c mice. No significant changes in body weight between the groups were observed during the period of treatment (Supporting information Fig. S12). The tumors of Hepes treated mice progressed rapidly. The tumor weight of mice treated with LT-DOX+LT-IMQ plus PD-L1 blockade was significantly lower than that of LT-DOX+LT-IMQ, LT-DOX and free drugs (Fig. 6A). As shown in Fig. 6B and C, LT-DOX+LT-IMQ group showed better anti-tumor efficiency than free drugs owing to the EPR and controlled release effects. Compared with LT-DOX-treated group, the combination of LT-DOX and LT-IMQ also significantly reduced the tumor volume ($P < 0.005$). Moreover, after combination with anti-PD-L1, LT-DOX+LT-IMQ further inhibited the tumor growth ($P < 0.01$ *vs.* LT-DOX+LT-IMQ group), which could be attributed to the reduced expression of PD-L1 and relieved immunosuppression.

H&E and TUNEL staining were used to further investigate the cell apoptosis in tumor (Fig. 6D). Tight nuclei of tumor cells were observed after treatment with Hepes, which was in accordance with the rapid tumor growth. In other groups, tumor tissues exhibited different degrees of apoptosis. Heart toxicity is a major

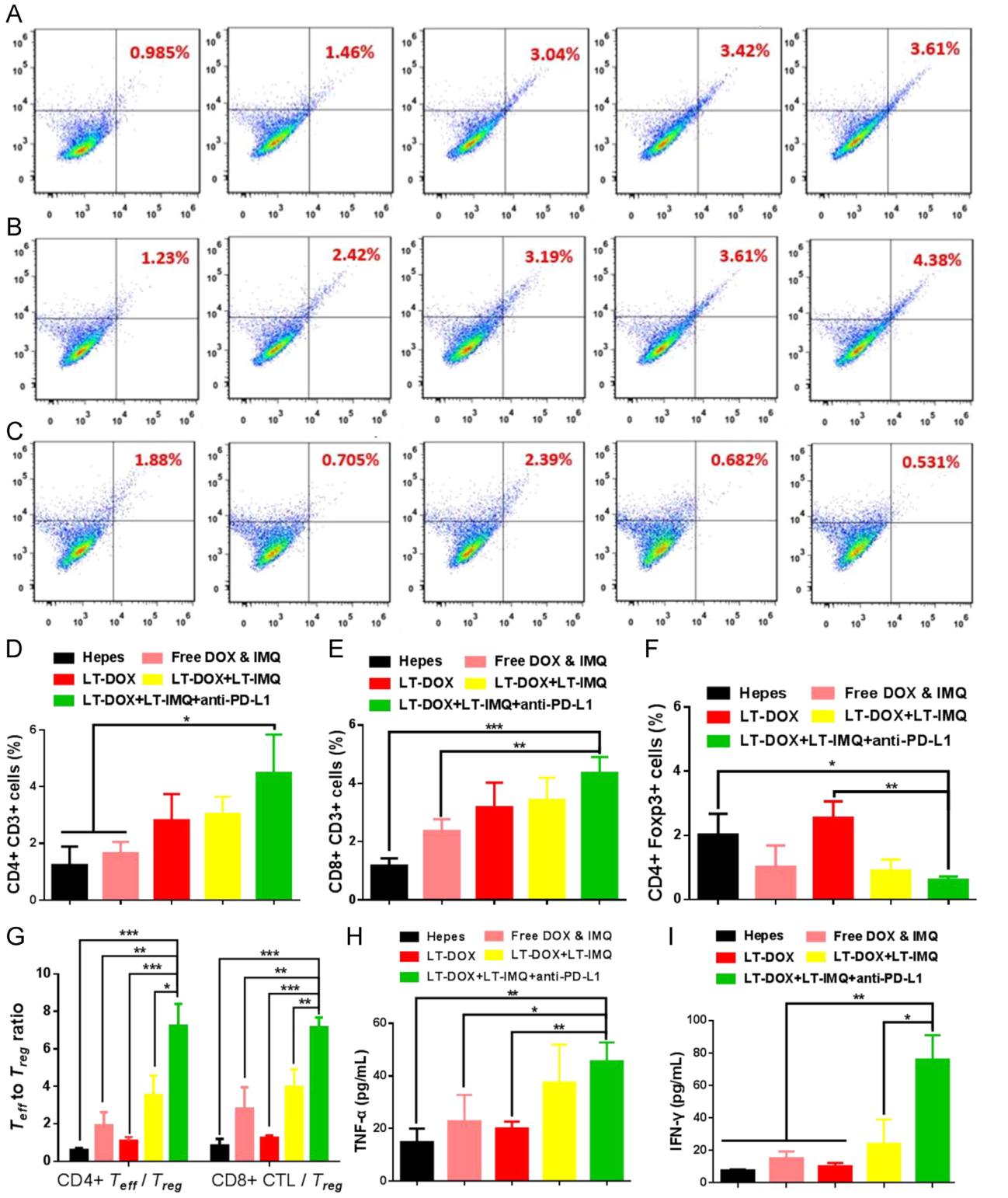

Figure 5 Representative flow cytometry plots showing percentages of tumor-infiltrating $CD3e^+CD4^+$ killer T cells (A), $CD3e^+CD8^+$ effector T cells (B) and $CD4^+FoxP3^+$ regulatory T cells (C) in solid tumors after various treatments indicated. From left to right are groups of Hepes, free DOX & IMQ, LT-DOX, LT-DOX+LT-IMQ, LT-DOX+LT-IMQ+anti-PD-L1. Proportions of $CD3e^+CD4^+$ effector T cells (C), $CD3e^+CD8^+$ T cells (D) and $CD4^+FoxP3^+$ regulatory T cells (E). (G) $CD4^+$CTLs/T_{reg} ratios and $CD8^+$ effector T cells/T_{reg} cells ratios in the solid tumors upon various treatments. Cytokine levels of TNF-α (H), and IFN-γ (I) in sera from mice isolated on day 3 after various treatments. Three mice were measured in each group in A–I. Data are mean $\pm$ SD, $n = 3$; $^{*}P < 0.05$; $^{**}P < 0.01$; and $^{***}P < 0.001$.

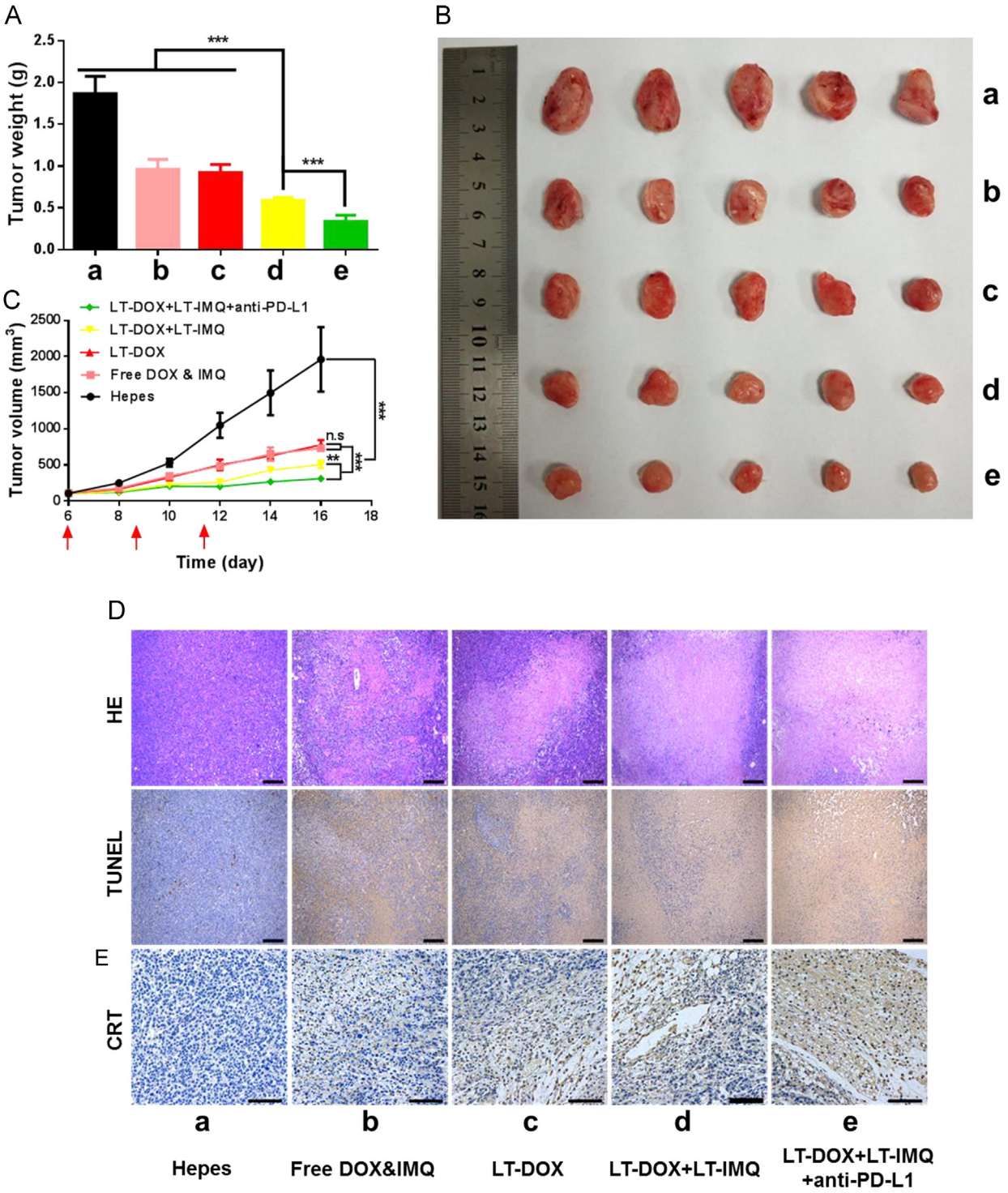

Figure 6 (A) The weights of dissected tumors at the end of treatment. (B) Tumor growth curves of 4T1 tumors when treated with different formulations. (C) Representative picture of tumors 16 days after implantation of 4T1 cells. (D) Representative H&E and TUNEL staining of tumor sections. The scale bar represents 200 μm. (E) Immunohistochemistry to detect CRT in tumors (shown in brown). The scale bar represents 100 μm. Data are mean ± SD, $n = 6$; $^{*}P < 0.05$; $^{**}P < 0.01$; and $^{***}P < 0.001$.

issue of DOX. No obvious heart toxicity was observed after loading DOX into the LT micelle (Supporting Information Fig. S14), suggesting this strategy decreased the toxicity of free DOX. Although LT-DOX+LT-IMQ had better anti-tumor effects than LT-DOX, PD-L1 expression was inevitably increased after treatment (Supporting Information Fig. S13), which indicated a bad prognosis. To block the immunosuppressive PD-1/PD-L1, anti-PD-L1 was used to down-regulate the expression of PD-L1. Immunohistochemical staining of tumors revealed a high level of CRT in DOX-treated mice. Unlike *in vitro* experiments, LT-DOX-treated group expressed more CRT than free drugs-treated group, because LT-DOX was more likely to reach the tumor site. Tumor

cells can degrade the stromal layer and then cross into the blood vessels by upregulating MMP9 expression, thereby forming a metastatic lesion at the distal end[44–46]. As shown in Supporting Information Fig. S15, compared with Hepes buffer and free drugs treated groups, the expression of MMP9 enzyme in groups treated with LT were reduced, inhibiting the metastasis of tumor cells. Therefore, LT-DOX+LT-IMQ plus anti-PD-L1 not only effectively inhibited the growth of solid tumor, but also inhibited the occurrence of *in situ* metastasis.

It is difficult to effectively treat metastatic tumors through traditional therapies such as surgery, chemotherapy and radiotherapy[47,48]. Several studies have reported that LMWH and TOS could reduce tumor metastasis in the mouse models[49]. Therefore, we wondered if LT-IMQ combine with LT-DOX could provide any opportunity in treating metastatic cancer. A relatively low dose of DOX was chosen for metastatic tumor treatment to reduce the anti-metastasis effect of DOX, but mainly investigate the role of anti-metastatic micelles LT. After 23 days of tumor inoculation, a large number of metastasized colonies were observed in lungs of Hepes-treated mice. Owing to the anti-metastatic effect of TOS and the enhanced accumulation in tumors, LT had a greater anti-metastatic ability than LMWH *in vivo*. Above all, LT-DOX+LT-IMQ plus PD-L1 blockade exhibited the strongest inhibition of tumor metastasis, showing minimum metastasis in lungs (Fig. 7C). Consistent with previous results, LT-DOX+LT-IMQ+anti-PD-L1 group exhibited the best anti-metastasis effect as indicated by H&E staining (Fig. 7D). Besides, immunohistochemical staining of lungs revealed that the expression of MMP9 enzyme in LT treated groups was reduced compared with the groups of Hepes, free drugs and LMWH (Fig. 7E).

These results demonstrated that LT-DOX+LT-IMQ combined PD-L1 blockade could not only suppress the orthotopic tumor, but also effectively inhibit the pulmonary metastasis of 4T1 cells, exhibiting potent anti-tumor effects.

4. Discussion

Chemo-immunotherapy has exhibited great potential in treatment of breast cancer and its metastasis. Chemotherapeutic drug DOX is essential for the treatment of a range of cancers, and has been demonstrated to activate tumor-specific immune responses[2,4,5]. In this study, DOX and immune adjuvant IMQ were chosen to activate powerful immune responses to treat cancers. PD-1 and PD-L1 are a

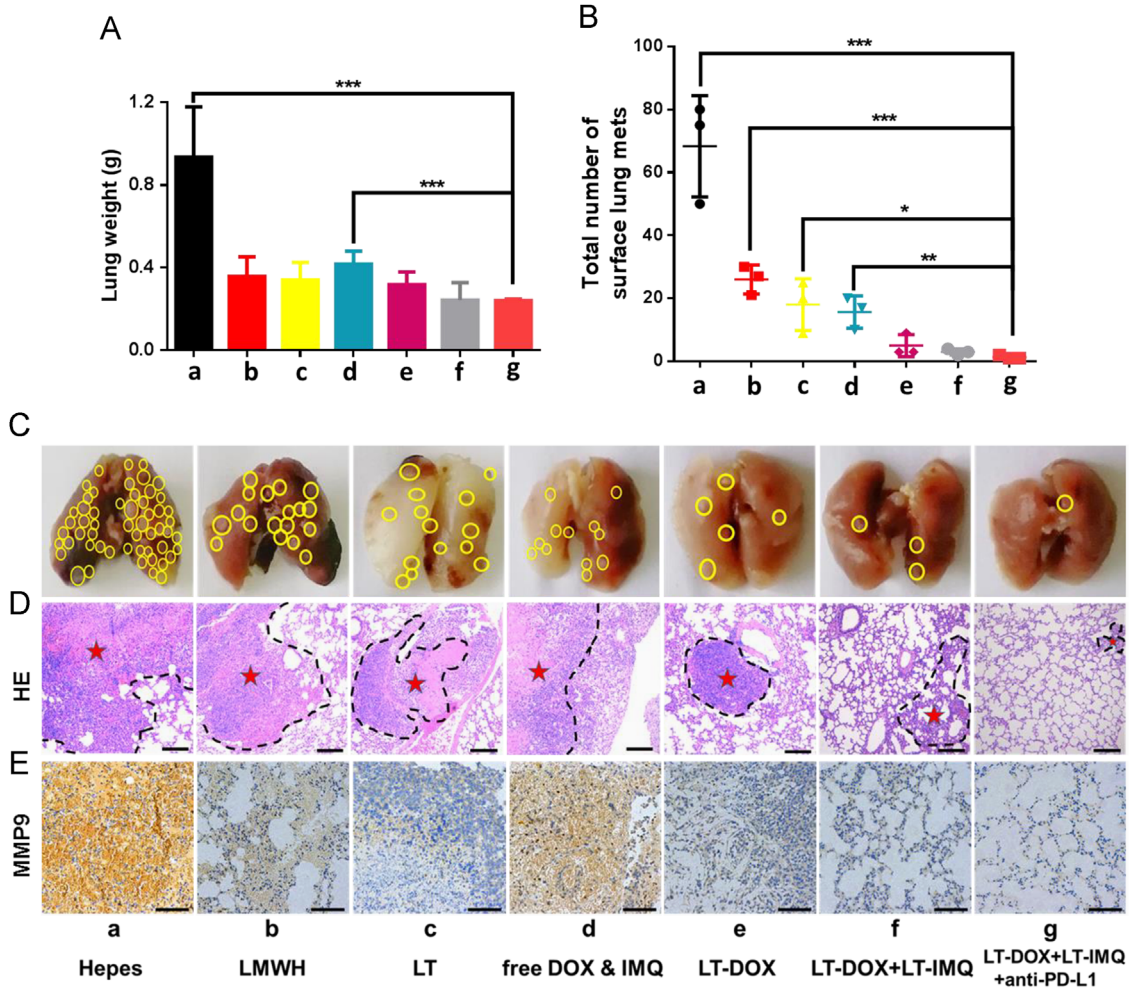

Figure 7 (A) The weights of lungs at the end of treatment. (B) Total number of surface lung Mets. (C) Representative pictures of lungs 23 days after injection of 4T1 cells *via* tail vein. The yellow circle represents the Mets. (D) Histological analysis of lung sections. The scale bar represents 200 μm. The dashed lines mean metastasis loci. (E) Immunohistochemistry to detect MMP9 in lung (shown in brown). The scale bar represents 100 μm. Data are mean ± SD, $n = 5$; $^{*}P < 0.05$; $^{**}P < 0.01$; and $^{***}P < 0.001$.

pair of important immunosuppressive molecules[50], which would attenuate the immune activation of DOX and IMQ. Thus, we used anti-PD-L1 to further elevate the immune responses.

Recently, because of excessive modification of nanoparticles, clinical applications have encountered with many obstacles[51]. In our latest study, we constructed a simple self-delivering micellar nanoparticle consisting of the anti-metastatic components LMWH and TOS, which inhibit different phases of the metastatic cascade[21]. Considering that the dosage of drugs can be adjusted more accurately, the drug-loaded micelles LT-DOX and LT-IMQ were formed. The two self-assembled micelles could prolong the circulation time and increase the accumulation in tumor through EPR effect. Flow cytometry, immunostaining analysis and immunohistochemical staining revealed a high level of CRT in LT-DOX-treated group. Then, the maturation of DCs and activation of tumor-specific immune responses of LT-DOX+LT-IMQ in combination with anti-PD-L1 were analyzed. The number of specific CTLs and secretion of IFN-γ and TNF-α were increased. The inhibitory PD-1/PD-L1 pathway has previously been demonstrated to limit the expansion of T_{reg} cells by controlling STAT-5 phosphorylation[52]. In the present manuscript, the number of T_{reg} cells was significantly reduced with PD-L1 blockade and the ratios of $CD8^+$ CTLs/T_{reg} cells and $CD4^+$ T_{eff}/T_{reg} cells of LT-DOX+LT-IMQ plus anti-PD-L1-treated group were increased by nearly 2-fold compared with LT-DOX+LT-IMQ-treated group, indicating stronger cellular immune responses in cancer immunotherapy.

Although many researches based on chemotherapeutics and immune adjuvant have entered clinical stage, it is rare that the researches deal with the combination of immunotherapy and chemotherapy to effectively treat metastatic 4T1 breast tumors. In this study, LMWH and TOS have good biocompatibility and anti-metastatic effect, which formed micelle in aqueous solution with good stability. Furthermore, LT could inhibit the adhesion between tumor cells and platelets and the production of MMP-9 to inhibit different stages of the metastasis cascade, so that the application of LT micelle to this immune activation strategy can strongly prevent metastasis. Wound healing assays, invasion assays and the treatment of lung metastasis of 4T1 breast cancer revealed a strong anti-metastasis effect of LT-DOX+LT-IMQ in combination with anti-PD-L1. MMP-9 is an enzyme secreted by various tumor cells, which can degrade extracellular matrix, promote cell detachment and invasion, and enhance tumor cells entry into blood vessels[53–55]. Immunostaining analysis of orthotopic and metastasis tumors indicated that the administration of micelles could reduce the secretion of MMP-9 in the tumor microenvironment. The anti-metastasis micelle LT was proven an efficient delivery system for chemo-immunotherapy of orthopotic and lung metastasis of breast cancer. In summary, we have rationally designed a multifunctional self-assembly micelle for enhanced chemo-immunotherapy. DOX loaded nanoparticles LT-DOX could initiate a tumor-specific immune response by eliciting immunogenic cell death (ICD), which further strengthened by adjuvant IMQ-loaded nanoparticles LT-IMQ. LT-DOX+LT-IMQ stimulate specific immune responses by triggering the maturation of DCs, increasing the number of specific CTLs and secretion of IFN-γ and TNF-α. Furthermore, the combination with clinically approved PD-L1 checkpoint blockade inhibited the activities of T_{reg} cells, which alleviated the immune inhibition signal and promoted anti-tumor efficacy. Our studies demonstrated that LT anti-metastatic micelle based chemo-immunotherapy strategy would be promising for orthotopic and metastatic breast cancer treatment.

Acknowledgments

The work was funded by the Major Projects of the National Natural Science Foundation of China (81690261), the National Natural Science Foundation of China (81703450) and the Postdoctoral Research Foundation of China (2017M620429).

Appendix A. Supporting information

Supporting data associated with this article can be found in the online version at https://doi.org/10.1016/j.apsb.2019.01.018.

References

1. Seigel R, Naishadham D, Jemal A. Cancer statistics, 2013. *CA Cancer J Clin* 2013;**63**:11–30.
2. Minotti G, Menna P, Salvatorelli E, Cairo G, Gianni L. Anthracyclines: molecular advances and pharmacologic developments in antitumor activity and cardiotoxicity. *Pharmacol Rev* 2004;**56**:185–229.
3. Shen N, Hu J, Zhang L, Zhang L, Sun Y, Xie Y, et al. Doxorubicin-loaded zein *in situ* gel for interstitial chemotherapy of colorectal cancer. *Acta Pharm Sin B* 2012;**2**:610–4.
4. Cook AM, Lesterhuis WJ, Nowak AK, Lake RA. Chemotherapy and immunotherapy: mapping the road ahead. *Curr Opin Immunol* 2015;**39**:23–39.
5. Noelia C, Pequignot MO, Antoine T, François G, Stéphan R, Nathalie C, et al. Caspase-dependent immunogenicity of doxorubicin-induced tumor cell death. *J Exp Med* 2005;**202**:1691–701.
6. Krysko DV, Garg AD, Kaczmarek A, Krysko O, Agostinis P, Vandenabeele P. Immunogenic cell death and DAMPs in cancer therapy. *Nat Rev Cancer* 2012;**12**:860–75.
7. Galluzzi L, Buqué A, Kepp O, Zitvogel L, Kroemer G. Immunogenic cell death in cancer and infectious disease. *Nat Rev Immunol* 2016;**17**:97–111.
8. Zitvogel L, Kepp O, Senovilla L, Menger L, Chaput N, Kroemer G. Immunogenic tumor cell death for optimal anticancer therapy: the calreticulin exposure pathway. *Clin Cancer Res* 2010;**16**:3100–4.
9. Wang Z, Zhang Y, Liu Z, Dong K, Liu C, Ran X, et al. A bifunctional nanomodulator for boosting CpG-mediated cancer immunotherapy. *Nanoscale* 2017;**9**:14236–47.
10. Obeid M. ERP57 membrane translocation dictates the immunogenicity of tumor cell death by controlling the membrane translocation of calreticulin. *J Immunol* 2008;**181**:2533–43.
11. Seth A, Heo MB, Lim YT. Poly(γ-glutamic acid) based combination of water-insoluble paclitaxel and TLR7 agonist for chemo-immunotherapy. *Biomaterials* 2014;**35**:7992–8001.
12. Nam J, Son S, Ochyl LJ, Rui K, Schwendeman A, Moon JJ. Chemo-photothermal therapy combination elicits anti-tumor immunity against advanced metastatic cancer. *Nat Commun* 2018;**9**:1074.
13. Kasturi SP, Skountzou I, Albrecht RA, Koutsonanos D, Hua T, Nakaya HI, et al. Programming the magnitude and persistence of antibody responses with innate immunity. *Nature* 2011;**470**:543–7.
14. Chen Q, Xu L, Liang C, Wang C, Peng R, Liu Z. Photothermal therapy with immune-adjuvant nanoparticles together with checkpoint blockade for effective cancer immunotherapy. *Nat Commun* 2016;**7**:13193.
15. Le MI, Poujol D, Sanlaville A, Sisirak V, Gobert M, Durand I, et al. Tumor promotion by intratumoral plasmacytoid dendritic cells is reversed by TLR7 ligand treatment. *Cancer Res* 2013;**73**:4629–40.
16. Ma F, Zhang J, Zhang J, Zhang C. The TLR7 agonists imiquimod and gardiquimod improve DC-based immunotherapy for melanoma in mice. *Cell Mol Immunol* 2010;**7**:381–8.
17. Nowak AK, Robinson BW, Lake RA. Gemcitabine exerts a selective effect on the humoral immune response: implications for combination chemo-immunotherapy. *Cancer Res* 2002;**62**:2353–8.

18. Adams M, Navabi H, Croston D, Coleman S, Tabi Z, Clayton A, et al. The rationale for combined chemo/immunotherapy using a Toll-like receptor 3 (TLR3) agonist and tumour-derived exosomes in advanced ovarian cancer. *Vaccine* 2005;**23**:2374–8.
19. Mei L, Liu Y, Zhang H, Zhang Z, Gao H, He Q. Antitumor and antimetastasis activities of heparin-based micelle served as both carrier and drug. *Acs Appl Mater Interfaces* 2016;**8**:9577–89.
20. Ling M, Liu Y, Xia C, Zhou Y, Zhang Z, Qin H. Polymer–drug nanoparticles combine doxorubicin carrier and heparin bioactivity functionalities for primary and metastatic cancer treatment. *Mol Pharm* 2017;**14**:513–22.
21. Yang L, Zhengze L, Ling M, Man L, Kebai R, Xuhui W, et al. Enhanced melanoma-targeted therapy by "Fru-blocked" phenyboronic acid-modified multiphase antimetastatic micellar nanoparticles. *Adv Sci* 2018;**0**:1800229.
22. Min Z, Altuwaijri S, Yeh S. RRR-α-tocopheryl succinate inhibits human prostate cancer cell invasiveness. *Oncogene* 2004;**23**:3080–8.
23. Youk HJ, Lee E, Choi MK, Lee YJ, Chung JH, Kim SH, et al. Enhanced anticancer efficacy of α-tocopheryl succinate by conjugation with polyethylene glycol. *J Control Release* 2005;**1**:43–52.
24. Lawson KA, Anderson K, Menchaca M, Atkinson J, Sun LZ, Knight V, et al. Novel vitamin E analogue decreases syngeneic mouse mammary tumor burden and reduces lung metastasis. *Mol Cancer Ther* 2003;**2**:437–44.
25. Zhang X, Peng X, Yu W, Hou S, Zhao Y, Zhang Z, et al. α-Tocopheryl succinate enhances doxorubicin-induced apoptosis in human gastric cancer cells *via* promotion of doxorubicin influx and suppression of doxorubicin efflux. *Cancer Lett* 2011;**307**:174–81.
26. Danhier F, Kouhé TT, Duhem N, Ucakar B, Staub A, Draoui N, et al. Vitamin E-based micelles enhance the anticancer activity of doxorubicin. *Int J Pharm* 2014;**1-2**:9–15.
27. Duhem N, Danhier F, Préat V. Vitamin E-based nanomedicines for anti-cancer drug delivery. *J Control Release* 2014;**182**:33–44.
28. Pardoll DM. The blockade of immune checkpoints in cancer immunotherapy. *Nat Rev Cancer* 2012;**12**:252–64.
29. Topalian SL, Drake CG, Pardoll DM. Immune checkpoint blockade: a common denominator approach to cancer therapy. *Cancer Cell* 2015;**27**:450.
30. Glennie MJ. Immunostimulatory monoclonal antibodies for cancer therapy. *Oncoimmunology* 2007;**7**:95–106.
31. Walter S, Weinschenk T, Stenzl A, Zdrojowy R, Pluzanska A, Szczylik C, et al. Multipeptide immune response to cancer vaccine IMA901 after single-dose cyclophosphamide associates with longer patient survival. *Nat Med* 2012;**18**:1254–61.
32. Mellman I, Coukos G, Dranoff G. Cancer immunotherapy comes of age. *Nature* 2011;**480**:480–9.
33. Zhao M, Guo W, Wu Y, Yang C, Zhong L, Deng G, et al. SHP2 inhibition triggers anti-tumor immunity and synergizes with PD-1 blockade. *Acta Pharm Sin B* 2018:610–4.
34. Köse GT, Arica MY, Hasirci V. Low-molecular-weight heparin-conjugated liposomes with improved stability and hemocompatibility. *Drug Deliv* 2009;**5**:257–64.
35. Proietti E, Moschella F, Capone I, Belardelli F. Exploitation of the propulsive force of chemotherapy for improving the response to cancer immunotherapy. *Mol Oncol* 2012;**6**:1–14.
36. Tesniere A, Panaretakis T, Kepp O, Apetoh L, Ghiringhelli F, Zitvogel L, et al. Molecular characteristics of immunogenic cancer cell death. *Cell Death Differ* 2008;**15**:3–12.
37. Bracci L, Schiavoni G, Sistigu A, Belardelli F. Immune-based mechanisms of cytotoxic chemotherapy: implications for the design of novel and rationale-based combined treatments against cancer. *Cell Death Differ* 2014;**21**:15–25.
38. Latchman SCLY Yvette E, Vijay K, Kuchroo GJF. PD-L1-deficient mice show that PD-L1 on T cells, antigen-presenting cells, and host tissues negatively regulates T cells. *Proc Natl Acad Sci U S A* 2004;**29**:10691–6.
39. Ge Y, Xi H, Ju S, Zhang X. Blockade of PD-1/PD-L1 immune checkpoint during DC vaccination induces potent protective immunity against breast cancer in hu-SCID mice. *Cancer Lett* 2013;**336**:253–9.
40. Neurath MF, Finotto S, Glimcher LH. The role of Th1/Th2 polarization in mucosal immunity. *Nat Med* 2002;**8**:567–73.
41. D'Elios M, Del Prete G. Th1/Th2 balance in human disease. *Transpl Proc* 1998;**30**:2373–7.
42. Gollnick SO, Vaughan L, Henderson BW. Generation of effective antitumor vaccines using photodynamic therapy. *Cancer Res* 2002;**62**:1604–8.
43. Korbelik M, Sun J, Cecic I. Photodynamic therapy-induced cell surface expression and release of heat shock proteins: relevance for tumor response. *Cancer Res* 2005;**65**:1018–26.
44. Friedl P, Wolf K. Tumour-cell invasion and migration: diversity and escape mechanisms. *Nat Rev Cancer* 2003;**3**:362–74.
45. Dirat B, Bochet L, Dabek M, Daviaud D, Dauvillier S, Majed B, et al. Cancer-associated adipocytes exhibit an activated phenotype and contribute to breast cancer invasion. *Cancer Res* 2011;**71**:2455–65.
46. Valastyan S, Weinberg RA. Tumor metastasis: molecular insights and evolving paradigms. *Cell* 2011;**147**:275–92.
47. Chen Q, Liang C, Wang X, He J, Li Y, Liu Z. An albumin-based theranostic nano-agent for dual-modal imaging guided photothermal therapy to inhibit lymphatic metastasis of cancer post surgery. *Biomaterials* 2014;**34**:9355–62.
48. Chen Q, Liang C, Wang C, Liu Z. An imagable and photothermal "Abraxane-like" nanodrug for combination cancer therapy to treat subcutaneous and metastatic breast tumors. *Adv Mater* 2015;**27**:903–10.
49. Borsig L, Wong R, Feramisco J, Nadeau DR, Varki NM, Varki A. Heparin and cancer revisited: mechanistic connections involving platelets, P-selectin, carcinoma mucins, and tumor metastasis. *Proc Natl Acad Sci U S A* 2001;**98**:3352–7.
50. Sharpe AH, Wherry EJ, Ahmed R, Freeman GJ. The function of programmed cell death 1 and its ligands in regulating autoimmunity and infection. *Nat Immunol* 2007;**8**:239–45.
51. Gao C, Zhang Y, Chen J, Wang T, Qian Y, Yang B, et al. Targeted drug delivery system for platinum-based anticancer drugs. *Mini Rev Med Chem* 2016;**16**:827–91.
52. Franceschini D, Paroli M, Francavilla V, Videtta M, Morrone S, Labbadia G, et al. PD-L1 negatively regulates $CD4^+CD25^+Foxp3^+$ Tregs by limiting STAT-5 phosphorylation in patients chronically infected with HCV. *J Clin Investig* 2009;**119**:551–64.
53. Steeg PS. Angiogenesis inhibitors: motivators of metastasis?. *Nat Med* 2003;**9**:822–3.
54. Bernhard EJ, Gruber SB, Muschel RJ. Direct evidence linking expression of matrix metalloproteinase 9 (92-kDa gelatinase/collagenase) to the metastatic phenotype in transformed rat embryo cells. *Proc Natl Acad Sci U S A* 1994;**91**:4293–7.
55. Cottam D, Rees R. Regulation of matrix metalloproteinases—their role in tumor invasion and metastasis. *Int J Oncol* 1993;**2**:861–72.